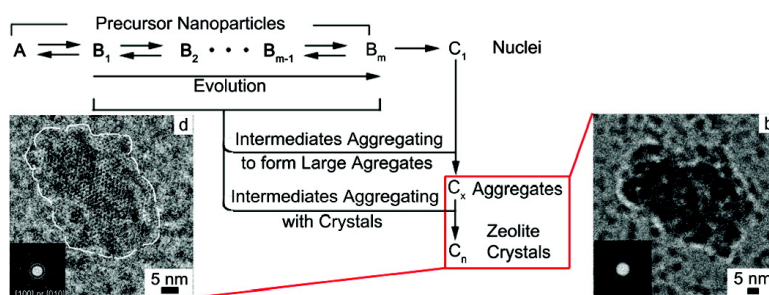Communication

A Structural Resolution Cryo-TEM Study of the Early Stages of MFI Growth

Sandeep Kumar, Zhuopeng Wang, R. Lee Penn, and Michael Tsapatsis

More About This Article

Additional resources and features associated with this article are available within the HTML version:

- Supporting Information
- Access to high resolution figures
- Links to articles and content related to this article
- Copyright permission to reproduce figures and/or text from this article

View the Full Text HTML

A Structural Resolution Cryo-TEM Study of the Early Stages of MFI Growth

Sandeep Kumar,[†,‡] Zhuopeng Wang,[†,§] R. Lee Penn,[‡] and Michael Tsapatsis*[,†]

*University of Minnesota, Department of Chemical Engineering and Materials Science, 151 Amundson Hall,
421 Washington Avenue SE, Minneapolis, Minnesota 55455, University of Minnesota, Department of Chemistry,
207 Pleasant Street SE, Minneapolis, Minnesota 55455, and Jilin University, State Key Laboratory of Inorganic
Synthesis and Preparative Chemistry, College of Chemistry, Changchun 130012, China*

Received August 19, 2008; E-mail: rleepenn@umn.edu; tsapatsi@cems.umn.edu

Understanding nucleation and growth phenomena in solution remains elusive partly due to the challenges involved in available sample preparation and characterization techniques. Such phenomena are of fundamental and practical significance for the synthesis of various materials including zeolites and other templated porous materials.[1−12] In this context, the synthesis of pure silica MFI (TPA-silicalite-1; hereafter referred to as MFI), in optically clear sols, has been studied extensively as a model system.[13−18] The synthesis mixture is prepared from tetraethylorthosilicate (TEOS), water, and tetrapropylammonium hydroxide (TPAOH). Upon hydrolysis of TEOS, nanoparticles with typical size ∼5 nm form spontaneously.[18] The nature of these nanoparticles and their role in early stages of MFI growth are still under debate.[18−20] Recently, we proposed a mechanism for the early stages of MFI growth.[21,22] It includes evolution of precursor nanoparticles to nuclei and crystal growth by aggregation of a fraction of the evolving nanoparticles (Figure 1). The precursor nanoparticles (denoted A) are known to initially have a disordered silica-core/TPA-shell structure.[16] We hypothesized that they evolve through intermediates (denoted B_1 to B_m) to nuclei C_1. A unique aspect of the proposed mechanism is that intermediate nanoparticles B_1 to B_m, although not yet fully transformed to MFI, can contribute to aggregation with different rates of attachment. This distributed population of nanoparticles, exhibiting diversity toward aggregative crystal growth,[21] was proposed to explain the prolonged induction period observed in MFI nucleation and the presence of relatively large crystals at low yield at the early stages of crystal growth. The proposed mechanism was based on the characterization of room temperature aged TPA-silica sol by a number of techniques such as atomic force microscopy (AFM), small-angle X-ray scattering (SAXS), and high-resolution transmission electron microscopy (HRTEM) and a phenomenological population balance mathematical model. Although room temperature aging may not be practical for commercial production of MFI, it enabled us to capture the complex steps involved in zeolite crystallization by ensuring slow evolution and avoiding complications that may be introduced during quenching before characterization. However, information regarding the structure of intermediate nanoparticles (B_1 to B_m), nuclei (C_1), and early aggregates (C_x) is still very limited since they are minor components of the sols at early stages of growth.

Here, we present a cryogenic transmission electron microscopy (cryo-TEM) study on sols, with a similar composition to those studied in ref 21, prior to and during the early stages of MFI formation. Cryo-TEM images with structural resolution are obtained and yield new insights in MFI growth. The TPA-silica sol used
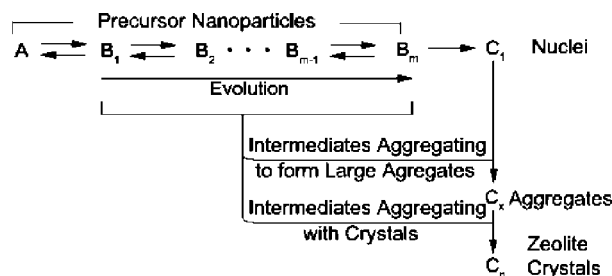

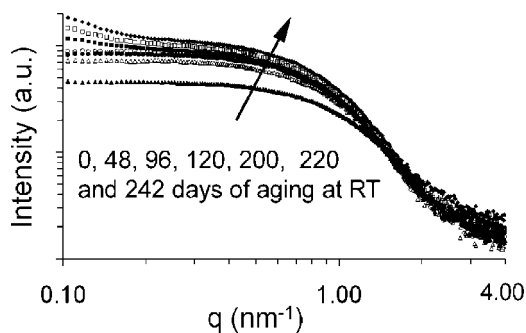**Figure 1.** Schematic illustrating the proposed growth mechanism.

Figure 2. SAXS scattering profiles from sols after various times at room temperature.

has a molar composition $20SiO_2/9TPAOH/9500H_2O/80C_2H_5OH$ and corresponds to a relatively small excess of silica beyond its solubility limit. It is one of the most dilute compositions that nucleates MFI and is used here because it is known to yield MFI crystals at room temperature over a reasonable time scale (i.e., ∼7 months). This slow time frame is ideal for attempting to discern structural differences in the evolving particles just before and during the early stages of crystal growth. At higher temperatures, the transition from isolated primary particles to MFI crystals occurs over days (ca. 40 °C) to hours (ca. 80 °C) for this silica sol composition. We believe that other more concentrated sols could also be studied using cryo-TEM to obtain images with structural resolution.

Before describing the results, we provide a brief description of difficulties in imaging at cryogenic temperature such as frost formation, film-thickness control, and specimen drift.[23−25] Frost formation during sample preparation (and transfer) is unavoidable but can be minimized by careful sample handling in a clean environment. Film thickness was controlled by adjusting the number of blots (by trial and error) and blot time. Specimen drift is caused by the temperature gradient around the specimen. Its affect can be minimized by adjusting exposure time and binning. Furthermore, zeolites are challenging materials to observe in TEM as they are

† University of Minnesota, Department of Chemical Engineering and Materials Science.
‡ University of Minnesota, Department of Chemistry.
§ Jilin University.
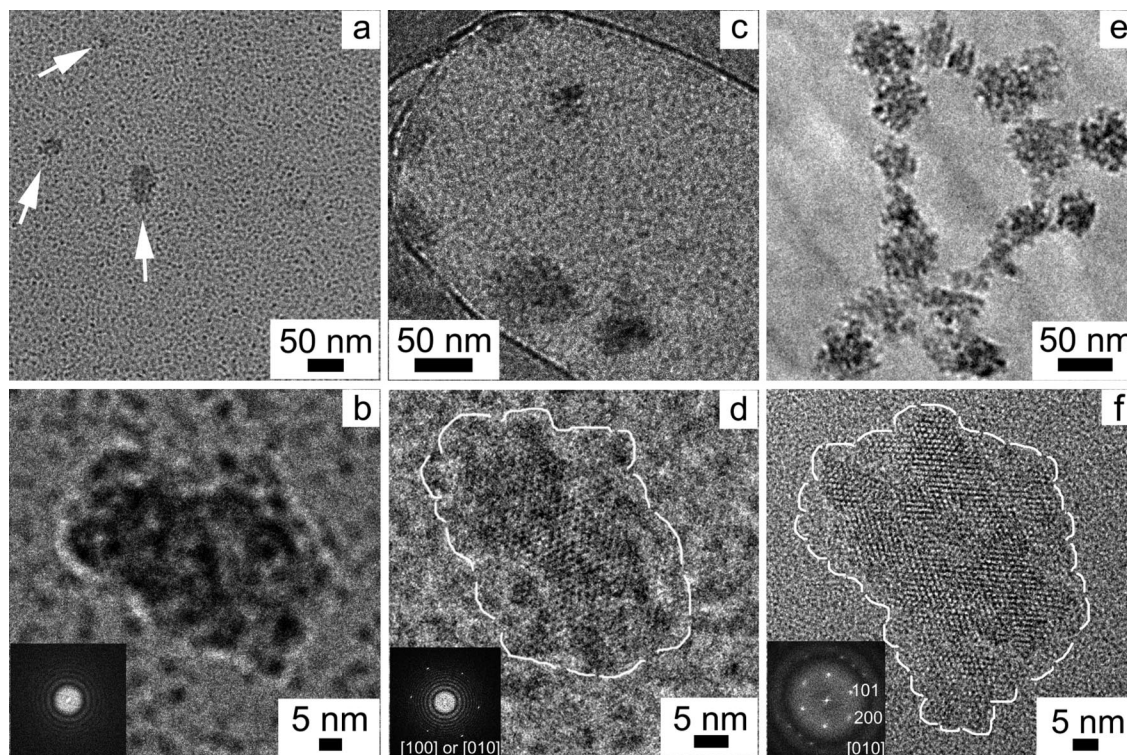
Figure 3. (a) A representative cryo-TEM image of the sol kept for 200 days at room temperature. A magnified image of a representative aggregate with FFT inset is shown in (b). (c) A cryo-TEM image of sol after 220 days; a high-resolution cryo-TEM image of a representative crystal with FFT inset is shown in (d). A cryo-TEM image of dialyzed sol after 220 days is shown in (e). A conventional (noncryogenic) TEM image of a dry crystal isolated from the dialyzed sol is shown in (f).
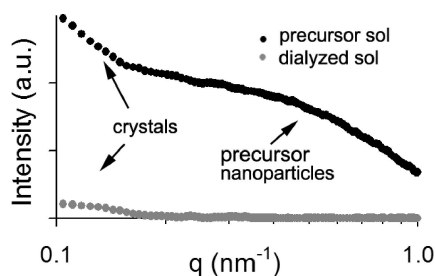
Figure 4. SAXS patterns from the original and dialyzed sols after 220 days at room temperature.

sensitive to the electron beam.[26−28] The electron dose to the specimen was kept to a minimum (by spreading the electron beam as much as practical) to minimize beam damage to MFI crystals. The binning and exposure time were optimized to gain adequate contrast while minimizing the effect due to drift. The imaging was performed at −178 °C using an FEI Tecnai G2 F30 TEM operated at 300 kV. The microscope has a twin-pole piece with a point-to-point resolution of 0.24 nm and enabled us to obtain images with structural resolution.

The detection of the onset of aggregation could be accomplished by DLS and/or SAXS.[21,29,30] Here we use SAXS because it can capture the very early stages of aggregation without uncertainties due to dust contamination and can effectively monitor the aggregate and precursor nanoparticle populations simultaneously. SAXS data (Figure 2) show the presence of ca. 5 nm precursor nanoparticles and the emergence of a second population of larger particles (evident by the rise in the low-q scattering intensity) after ∼200 days, in agreement with the previous report.[21] Representative cryo-TEM data of the sols after the detection of larger particles (200 days) are shown in Figure 3a. A small number (by comparison to precursor nanoparticles) of aggregate-like larger particles (30−50 nm), indicated by arrows, are present in a sea containing dark dots (contrast due to the ca. 5 nm precursor nanoparticles). The magnified image of an aggregate is shown in Figure 3b. The Fast Fourier Transform (FFT), shown in the inset, shows no evidence for crystallinity in these aggregate-like particles. No evidence of crystallinity was observed in 20 such aggregates that were examined. Their stability under the beam suggests that these features are not artifacts due to surface contamination but rather the silica particles responsible for the low q scattering intensity in the SAXS data. This was also suggested by the location of these particles inside the vitrified sol rather than on its surface. We conclude that the larger particles detected by SAXS (here, after 200 days) and denoted by C_x in Figure 1 are predominantly amorphous. This new finding could not be obtained in our previous work employing conventional (noncryogenic) TEM and dialysis for sample preparation because, most likely, the aggregates dissolved during dialysis.[21]

A representative cryo-TEM image of the sol after 220 days is shown in Figure 3c. Again, as expected from the SAXS data, larger particles as well as precursor nanoparticles are present. In contrast to the aggregates observed in specimens collected after 200 days, the aggregates observed at 220 days exhibit lattice fringes consistent with the MFI crystal structure (Figure 3d). White lines serve to highlight the crystal perimeter and indicate the absence of well developed facets. The FFT (inset of Figure 3d) indicates that the crystal is oriented along either the [100]- or [010]-axis, with the dots inside the highlighted perimeter representing the sinusoidal or straight MFI channels. Ten of such particles were closely inspected. To our knowledge, this is the first time such resolution has been achieved for zeolites imaged in the parent sol by cryo-TEM. The crystals do not have the typical MFI morphology. Instead they are aggregate-like and are in the similar size range (∼30−50

nm) as the predominantly amorphous aggregates shown in Figure 3a−b. This observation suggests that the particles observed at ∼200 days continue to transform and give rise to MFI crystals sometime between 200 and 220 days (a relatively short period). This observation adds a new element to the aggregation mechanism we have proposed before (Figure 1) in that early aggregates (C$_x$) do not have, to say the least, a well developed MFI structure. The transformation takes place in a relatively short period of time. However, we cannot state if it is a sudden or gradual transformation or if it is taking place simultaneously or starts localized and propagates through the particle. More in-depth studies with improved time resolution as well as sol characterization by other techniques, such as nuclear magnetic resonance (NMR),[31] mass spectroscopy (MS),[32] and infrared spectroscopy (IR),[33] are required to further elucidate the zeolite nucleation events.

One of the challenges faced in the present work was due to very low aggregate and crystal yield (<5%) imposed by our desire to observe the very first nucleation and growth events. The low aggregate and crystal yield made it difficult to find particles other than the 5 nm precursor nanoparticles on the TEM grid. Furthermore, high-resolution imaging requires an incident electron beam on a relatively smaller area of the sample. So, there is a fair chance that while imaging a certain crystallite, other nearby ones are amorphized. Therefore, although we can state with certainty the presence of only predominantly amorphous aggregates in 200 days, we cannot make similar strong statements regarding the coexistence of amorphous with crystalline aggregate-like particles in 220 day aged sols.

We further examined the sols containing MFI crystals (220 days) after using a dialysis procedure previously reported[21] so as to isolate MFI crystals from precursor nanoparticles and dissolved species. SAXS patterns from the original and dialyzed sol are shown in Figure 4. A representative cryo-TEM image from the dialyzed sol is shown in Figure 3e. The SAXS pattern agrees with the cryo-TEM observation; i.e., only the larger particles are present in the dialyzed sol. Moreover, crystals in the dialyzed sol exhibit characteristic swiss-cheese morphology, while voids are not evident in the crystals present in the original sol. For comparison, a high-resolution conventional (noncryogenic) TEM image of a (dry) crystal isolated from the dialyzed sol is shown in Figure 3f. White lines serve to highlight the crystal perimeter. The FFT, shown in the inset, shows that the crystal is oriented along the [010]-axis. We attribute the voids created by dialysis to the dissolution of partially transformed regions distributed within the crystals. SAXS may not detect a change in the particles due to the formation of such voids because the overall size and shape of the postdialysis crystals is similar to those of the predialysis aggregates. In this respect, the statement we made in ref 21 "SAXS analysis indicated that the crystals are not affected significantly by the dialysis procedure" is not precise as now we have clear evidence that dialysis results in the partial dissolution of the aggregates. However, the presence of such regions is in agreement with the mechanism proposed in ref 21: aggregative MFI growth by attachment of ∼5 nm nanoparticles that do not have a well developed structure.[21]

The importance of this study is twofold. First, it provides evidence supporting the recently proposed mechanism of evolution of nanoparticles followed by aggregative crystal growth while adding a new element. The new element, not included in the previously proposed model, is the formation of predominantly amorphous aggregates before MFI crystallization and points to the importance of intra-aggregate rearrangements in nucleation and growth.[7,34] Second, it demonstrates that, in addition to metal nanoparticles,[35] electron-beam sensitive materials such as zeolites can be imaged by cryo-TEM with structural resolution in their parent sols. Similar studies for other zeolites under different conditions may reveal useful structural information for the understanding of hydrothermal nucleation and growth.

Supporting Information Available: Details of experimental procedures. This material is available free of charge via the Internet at http://pubs.acs.org.

References

(1) Tsapatsis, M. *AIChE J.* **2002**, *48* (4), 654.
(2) Davis, M. E. *Nature* **2002**, *417*, 813.
(3) Lai, Z.; Tsapatsis, M.; Nicolich, J. P. *Adv. Funct. Mater.* **2004**, *14* (7), 716.
(4) Bonilla, G.; Vlachos, D. G.; Tsapatsis, M. *Microporous Mesoporous Mater.* **2001**, *42*, 191.
(5) Snyder, M.; Tsapatsis, M. *Angew. Chem., Int. Ed.* **2007**, *46*, 7560.
(6) Wang, J.; Vinu, A.; Coppens, M. O. *J. Mater. Chem.* **2007**, *17*, 4265.
(7) Mintova, S.; Olson, D. H.; Valtchev, V.; Bein, T. *Science* **1999**, *283*, 958.
(8) Valtchev, V.; Bozhilov, N. *J. Am. Chem. Soc.* **2005**, *127*, 16171.
(9) Li, S.; Li, Z.; Bozhilov, K. N.; Chen, Z.; Yan, Y. *J. Am. Chem. Soc.* **2004**, *126*, 10732.
(10) Schuth, F. *Curr. Opin. Solid State Mater. Sci.* **2001**, *5* (5), 389.
(11) Ruthstein, S.; Schmidt, J.; Kesselman, E.; Talmon, Y.; Goldfarb, D. *J. Am. Chem. Soc.* **2006**, *128*, 3366.
(12) Ruthstein, S.; Schmidt, J.; Kesselman, E.; Popovitz-Biro, R.; Omer, L.; Frydman, V.; Talmon, Y.; Goldfarb, D. *Chem. Mater.* **2008**, *20*, 2779.
(13) Rimer, J. D.; Trofymluk, O.; Navrotsky, A.; Lobo, R. F.; Vlachos, D. G. *Chem. Mater.* **2007**, *19*, 4189.
(14) de Moor, P. E. A.; Beelen, T. P. M.; Komanschek, B. U.; Diat, O.; Santen, R. A. V. *J. Phys. Chem. B* **1997**, *101*, 11077.
(15) Agger, J. R.; Hanif, N.; Cundy, C. S.; Wade, A. P.; Dennison, S.; Rawlison, P. A.; Anderson, M. W. *J. Am. Chem. Soc.* **2003**, *125*, 830.
(16) Fedeyko, J. M.; Rimer, J. D.; Lobo, R. F.; Vlachos, D. G. *J. Phys. Chem. B* **2004**, *108*, 12271.
(17) Cheng, C.-H.; Shantz, D. F. *J. Phys. Chem. B* **2005**, *109*, 13912.
(18) Schoeman, B. J.; Regev, O. *Zeolites* **1996**, *17*, 447.
(19) Ramanan, H.; Kokkoli, E.; Tsapatsis, M. *Angew. Chem., Int. Ed.* **2004**, *43*, 2.
(20) Liang, D.; Follens, L. R. A.; Aerts, A.; Martens, J. A.; Van Tendeloo, G. *J. Phys. Chem. C* **2007**, *111* (39), 14283.
(21) Davis, T. M.; Drews, T. O.; Ramanan, H.; He, C.; Dong, J.; Schnablegger, H.; Katsoulakis, M. A.; Kokkoli, E.; McCormick, A. V.; Penn, R. L.; Tsapatsis, M. *Nat. Mater.* **2006**, *5*, 400.
(22) Kumar, S.; Davis, T. M.; Ramanan, H.; Penn, R. L.; Tsapatsis, M. *J. Phys. Chem. B* **2007**, *111*, 3398.
(23) Talmon, Y. *Colloids Surf.* **1986**, *19*, 237.
(24) Bellare, J. R.; Davis, H. T.; Scriven, L. E.; Talmon, Y. *J. Electron Microsc.* **1988**, *10*, 87.
(25) Talmon, Y. *J. Colloid Interface Sci.* **1983**, *93* (2), 366.
(26) Pan, M. *Micron* **1996**, *27* (3−4), 219.
(27) Thomas, J. M.; Terasaki, O.; Gai, P. L.; Zhou, W.; Gonzalez-Calbet, J. *Acc. Chem. Res.* **2001**, *34*, 583.
(28) Treacy, M. M. J.; Newsam, J. M. *Ultramicroscopy* **1987**, *23* (3−4), 411.
(29) Mintova, S.; Olson, N. H.; Senker, J.; Bein, T. *Angew. Chem., Int. Ed.* **2002**, *41* (14), 2558.
(30) Cheng, C.-H.; Shantz, D. F. *Curr. Opin. Colloid Interface Sci.* **2005**, *10*, 188.
(31) Epping, J. D.; Chmelka, B. F. *Curr. Opin. Colloid Interface Sci.* **2006**, *11*, 81.
(32) Pelster, S. A.; Schrader, W.; Schuth, F. *J. Am. Chem. Soc.* **2006**, *128*, 4310.
(33) Patis, A.; Dracopoulos, V.; Nikolakis, V. *J. Phys. Chem. C* **2007**, *111*, 17478.
(34) Tsapatsis, M.; Lovallo, M.; Davis, M. E. *Microporous Mater.* **1996**, *5*, 381.
(35) Balmes, O.; Malm, J. O.; Pettersson, N.; Karlsson, G.; Bovin, J. O. *Microsc. Microanal.* **2006**, *12*, 1.

JA8063167